The EMBO Journal Vol.16 No.23 pp.6936–6946, 1997

Solution structure of midkine, a new heparin-binding growth factor

Wakana Iwasaki[1,2], Koji Nagata[1], Hideki Hatanaka[1], Tatsuya Inui[3], Terutoshi Kimura[3], Takashi Muramatsu[4], Keiichi Yoshida[5], Mitsuo Tasumi[2] and Fuyuhiko Inagaki[1,6]

[1]Tokyo Metropolitan Institute of Medical Science, 3-18-22, Honkomagome, Bunkyo-ku Tokyo 113, [2]Department of Chemistry, Graduate School of Science, University of Tokyo, 7-3-1, Hongou, Bunkyo-ku, Tokyo 113, [3]Peptide Institute Inc., 4-1-2, Ina, Minoh, Osaka 562, [4]Department of Biochemistry, Nagoya University School of Medicine, 65, Tsurumai-cho, Showa-ku, Nagoya 466 and [5]Tokyo Research Institute, Seikagaku Corporation, 3-1253, Tateno, Higashiyamato, Tokyo 207, Japan

[6]Corresponding author
e-mail: inagaki@rinshoken.or.jp

Midkine (MK) is a 13 kDa heparin-binding polypeptide which enhances neurite outgrowth, neuronal cell survival and plasminogen activator activity. MK is structurally divided into two domains, and most of the biological activities are located on the C-terminal domain. The solution structures of the two domains were determined by NMR. Both domains consist of three antiparallel β-strands, but the C-terminal domain has a long flexible hairpin loop where a heparin-binding consensus sequence is located. Basic residues on the β-sheet of the C-terminal domain form another heparin-binding site. Measurement of NMR signals in the presence of a heparin oligosaccharides verified that multiple amino acids in the two sites participated in heparin binding. The MK dimer has been shown to be the active form, giving signals to endothelial cells and probably to neuronal cells. We present a head-to-head dimer model of MK. The model was supported by the results of cross-linking experiments using transglutaminase. The dimer has a fused heparin-binding site at the dimer interface of the C-terminal domain, and the heparin-binding sites on MK fit the sulfate group clusters on heparin. These features are consistent with the proposed stronger heparin-binding activity and biological activity of the dimer.

Keywords: dimerization/growth factor/heparin binding/midkine/three-dimensional structure

Introduction

Growth factors, which play fundamental roles in regulation of growth, differentiation and development, frequently bind to extracellular matrices, especially heparin-like carbohydrates of heparan sulfate proteoglycans (Lindhal *et al.*, 1991; Ruoslahti and Yamaguchi, 1991). This property is helpful in storage of the factors in proper sites and their controlled release. Furthermore, binding of fibroblast growth factor (FGF) to cell surface heparan sulfate proteoglycans causes its oligomerization (Spivak-Kroizman *et al.*, 1994), which is essential for receptor binding and activation (Yayon *et al.*, 1991; Spivak-Kroizman *et al.*, 1994).

Midkine (MK) is a new heparin-binding growth factor of 13 kDa, and its expression is controlled by retinoic acid (Kadomatsu *et al.*, 1988; Tomomura *et al.*, 1990). MK, which is rich in basic amino acids and cysteines, has 45% sequence identity with heparin-binding growth-associated molecule (HB-GAM, also called pleiotrophin, PTN) (Li *et al.*, 1990; Merenmies and Rauvala, 1990). Retinoic acid-inducible heparin-binding protein isolated from chicken embryos has 65% sequence identity with MK, and is probably the chicken counterpart of MK (Raulais *et al.*, 1991). They are structurally unrelated to other proteins and form a new growth factor family (Figure 1A) (Muramatsu, 1994; Kurtz *et al.*, 1995).

MK expression is strong in embryonic periods, especially in the midgestation stage (Kadomatsu *et al.*, 1990; Mitsiadis *et al.*, 1995a,b). The nerve tissues, epithelial tissues and mesoderm tissues undergoing remodeling are the sites where MK expression is most intense. The functional role of MK has been best clarified in the nervous system. MK enhances survival and neurite outgrowth of embryonic neurons, and promotes neuronal differentiation (Michikawa *et al.*, 1993a,b; Muramatsu *et al.*, 1993). MK in the cerebral cortex of 17 day rat embryos is located on the radial glial process along which neurons migrate (Matsumoto *et al.*, 1994). HB-GAM promotes neurite outgrowth (Rauvala, 1989) and, furthermore, is involved in postsynaptic induction (Peng *et al.*, 1995).

MK is also known to promote plasminogen activator activity in bovine aortic endothelial cells, leading to increased fibrinolysis (Kojima *et al.*, 1995a). This activity forms a part of the basis of the retinol-induced increase of fibrinolytic activity of endothelial cells.

Recent studies revealed the medical significance of this new growth factor family. MK mRNA expression is increased in various human carcinomas (Tsutsui *et al.*, 1993; Aridome *et al.*, 1995). In neuroblastomas and bladder carcinomas, strong expression of MK in the tumor correlates with a worse prognosis for the patients (Nakagawa *et al.*, 1995; O'Brien *et al.*, 1996). Transfection of HB-GAM cDNA or MK cDNA into NIH-3T3 cells results in oncogenic transformation (Chauhan *et al.*, 1993; Kadomatsu *et al.*, 1997). MK has been identified recently as a target gene of the Wilm's tumor suppression gene (Adachi *et al.*, 1996). On the other hand, HB-GAM has been shown to be a tumor-derived angiogenic factor, and ribozyme targeting of the factor resulted in suppression of invasion and metastasis of melanoma and choricarcinoma (Czubayko *et al.*, 1996; Schulte *et al.*, 1996). Furthermore, MK accumulates in senile plaques of the brain of

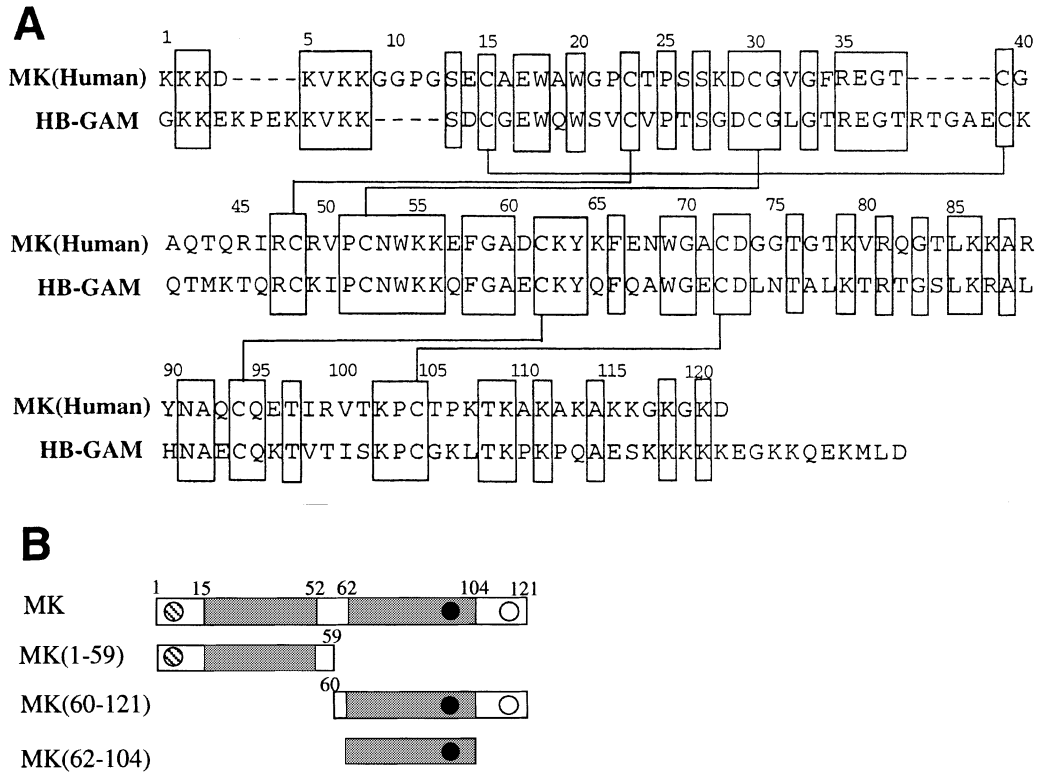

Fig. 1. (**A**) Amino acid sequences of MK and HB-GAM. Conserved amino acids are boxed. MK and HB-GAM have ~50% sequence identity, and all the disulfide bonds are conserved. (**B**) Schematic diagram of MK, MK(1–59), MK(60–121) and MK(62–104). The regions flanked by intradomain disulfide bridges are colored in gray. ● and ○, heparin-binding consensus sequences. ▨ , a sequence similar to the consensus sequence ▨ , KKDKV; ●, LKKARY; ○, AKKGKG).

Alzheimer's disease patients. MK is expressed in the edema region upon experimental brain infarction at as early as 1 day after operation (Yoshida *et al.*, 1995). Destruction of the retinal nuclear outer layer by exposure to constant light is prevented by MK administration (Unoki *et al.*, 1994). MK and HB-GAM are likely to be important molecules involved in tissue repair, and their aberrant expression occurs in diseases.

So far nothing is known about the three-dimensional (3D) structure of MK or HB-GAM. The following three interesting characteristics of MK prompted us to elucidate the 3D structure. Firstly, MK is composed of two domains [the N-terminally located domain, MK(15–52), and the C-terminally-located domain, MK(62–104)] flanked by intradomain disulfide bridges (Figure 1B) (Fabri *et al.*, 1993). This unique domain structure is conserved in HB-GAM (Fabri *et al.*, 1992). The C-terminal half of MK(60–121) was found to retain neurite outgrowth-promoting activity (Muramatsu *et al.*, 1994) and plasminogen activator-enhancing activity (Kojima *et al.*, 1995b). Furthermore, MK(62–104) retains the latter activity, and this is the smallest peptide so far reported to be capable of inducing the fibrinolytic activity (Kojima *et al.*, 1995b). Both MK and HB-GAM bind strongly to syndecans, cell surface heparan sulfate proteoglycans (Raulo *et al.*, 1994; Mitsiadis *et al.*, 1995a). N-Syndecan has been proposed to be the receptor for HB-GAM upon HB-GAM-induced neurite outgrowth (Raulo *et al.*, 1994). A low dose of heparin inhibits neurite outgrowth activity of both HB-GAM (Raulo *et al.*, 1994; Kinnunen *et al.*, 1996) and MK (Kaneda *et al.*, 1996a,b). Thus, recognition of heparin by MK(62–104) is involved at least in neurite outgrowth promotion by the factors. Elucidation of the 3D structure of this functionally important heparin-binding domain may provide information concerning the specificity of heparin–protein interactions. Secondly, MK is a heat- and acid-stable growth factor, and heating at 97°C for 5 min or treatment with 1 M HCl at room temperature do not significantly affect plasminogen activator-enhancing activity nor neurite outgrowth-promoting activity (Kojima *et al.*, 1995c). Thus, it is of interest to determine the basis of this unusual stability from a structural view point. Thirdly, MK is known to cross-link to form a dimer by the action of transglutaminase (Kojima *et al.*, 1995a), and heparin promotes MK dimerization (Kojima *et al.*, 1997). Recent studies have shown that this dimerization enhances plasminogen activator activity (Kojima *et al.*, 1997) and regulation of neuronal cell migration (Mahoney *et al.*, 1996). The 3D structure of MK is expected to shed light on the functionally important complex of the MK dimer and heparin-like carbohydrates.

Results

NMR analysis of MK, MK(1–59), MK(60–121) and MK(62–104)

We attempted to assign NMR resonances of MK, MK(1–59), MK(60–121) and MK(62–104) to individual protons in a sequence-specific manner using the sequential assignment method (Wüthrich, 1986). First, NMR resonances were assigned to the spin systems of specific amino acid types by using double-quantum filtered correlation

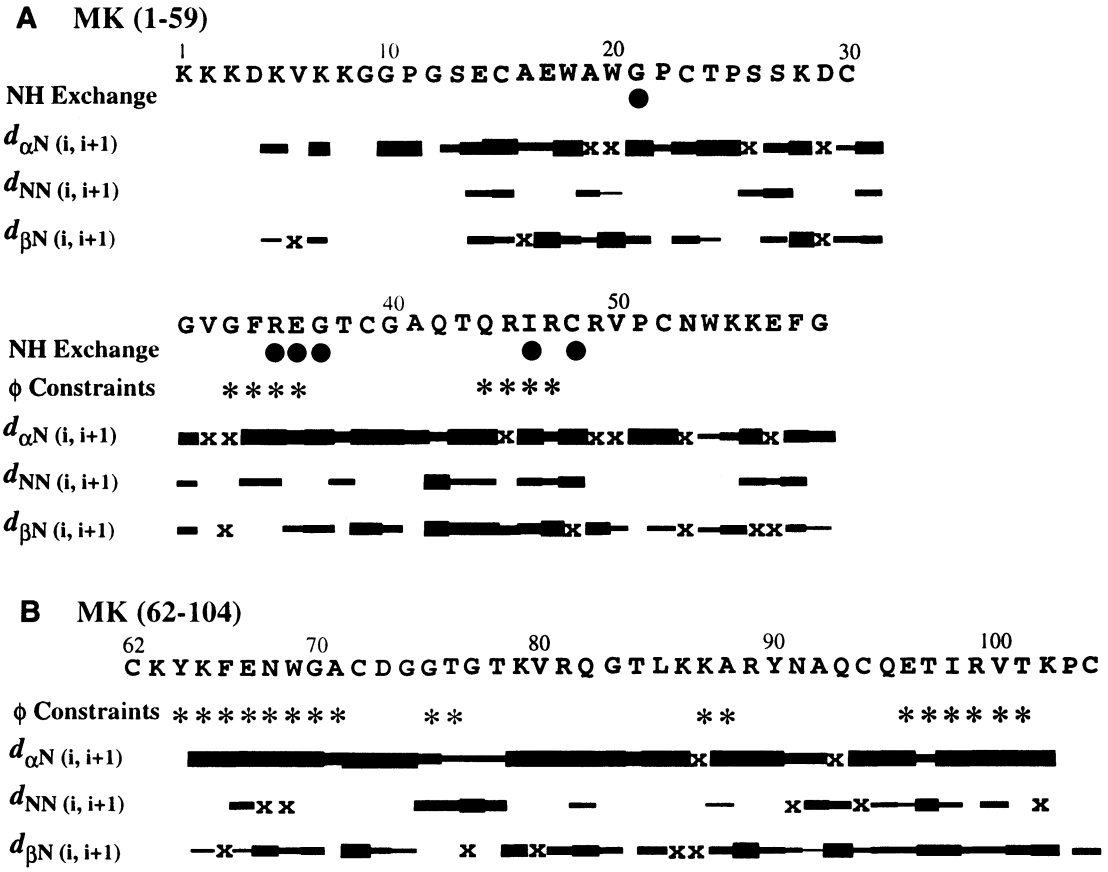

Fig. 2. Sequential NOE connectivities in (**A**) MK(1–59) and (**B**) MK(62–104). The height of the bars indicates the approximate intensity of the NOESY cross-peaks recorded with a mixing time of 75 and 100 ms, respectively. x indicates an NOE connectivity which is not assigned due to overlap with other NOE peaks. Filled circles and asterisks indicate slowly exchanging NH protons and dihedral angle (φ) constraints.

spectroscopy (DQF-COSY) and total correlation spectroscopy (TOCSY). Secondly, the spin systems were aligned according to the sequence using sequential connectivities obtained by nuclear Overhauser effect (NOE) spectroscopy (NOESY) experiments. However, several C-terminal tail lysine residues in MK and MK(60–121) could not be assigned due to overlap of signals or bleaching of amide proton resonances by solvent pre-saturation. Since 13 amino acid residues in the C-terminal tail (109–121) have no biological functions except for antigenicity (Muramatsu *et al.*, 1994), we concentrated our efforts on MK(1–59) and MK(62–104). We established the complete sequence-specific resonance assignments of these peptides and revealed the sequential NOE connectivities (Figure 2). Successive strong long-range NOE connectivites between C^{α}Hs were observed. These NOEs are characteristic of the pairs of C^{α}Hs located on the opposite strands of the antiparallel β-sheet. Thus, we determined the alignment of the β-strands and confirmed the secondary structures of MK(1–59) and MK(62–104) as shown in Figure 3. We also confirmed that the secondary structure found in MK(62–104) was also retained in MK(60–121). In these peptides, all Pro residues were connected to the preceding residues by C^{α}H (i) – C^{δ}H (i+1) connectivity ($d_{\alpha\delta}$), indicating that Pro residues take the *trans* configuration.

MK is divided into two halves, MK(1–59) and MK(60–121). The NOESY spectrum of MK could be interpreted essentially by the superposition of those of MK(1–59) and MK(60–121) (Figure 4), suggesting that these halves are relatively independent. As the NOE peaks characteristic of the triple-stranded β-sheet structure in each MK(1–59) and MK(60–121) were almost identical with those in MK, we concluded that the domain structures in the individual halves were maintained in MK. Phe55 in mouse MK (Phe58 in human MK) was susceptible to chymotryptic digestion (Matsuda *et al.*, 1996), indicating that the linker was exposed. Although the chemical shift differences were conspicuous for Asn53–Lys55, Trp69, Thr84–Lys86, Ala88–Tyr90, Ala92 and Ile98–Arg99, they were <0.05 p.p.m. Both the N- and C-terminal halves in MK would exist essentially independently and resemble closely those of MK(1–59) and MK(60–121). Since MK(62–104) has almost full biological activity in terms of fibrinolytic activity, its structural determination is significant for elucidating the function of MK.

Tertiary structure of MK(1–59) and MK(62–104)

The 3D structures of MK(1–59) and MK(62–104) were determined by the simulated annealing method (YASAP) with XPLOR v3.1 using distance constraints derived from the NOESY experiments, the hydrogen bonds and the disulfide bonds. A total of 100 calculations were carried out, and a final set of 20 structures was selected on the basis of agreement with the experimental constraints and van der Waals energy. The structural statistics are shown in Table I. The number of NOESY distance connectivities

and the root mean square deviations (r.m.s.ds) from the mean structures of each residue for MK(1–59) (Figure 5A) and MK(62–104) (Figure 5B) are shown. The structure

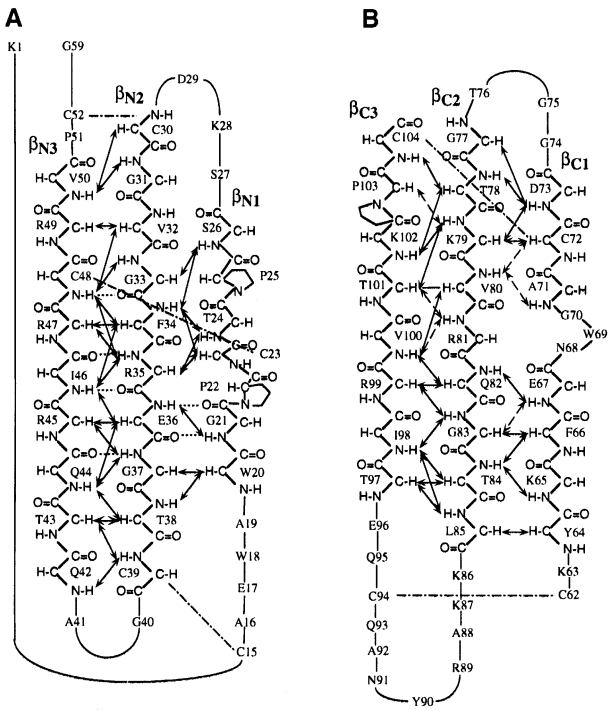

Fig. 3. Secondary structures of (**A**) MK(1–59) and (**B**) MK(62–104) identified with interstrand backbone NOE connectivities (arrows). Chain and dotted lines represent disulfide bonds and hydrogen bonds as manifested by amide proton exchange rates, respectively. Broken arrows indicate expected but unassigned NOEs either due to overlap with other NOE peaks or due to bleaching by water suppression.

was well defined, except for the terminal region (Lys1–Ser13 and Asn53–Gly59) and the loops (Gly74–Thr76 and Lys86–Gln93). The r.m.s.d.s between the 20 structures and the mean structures were 0.88 ± 0.23 Å [MK(1–59)] and 1.05 ± 0.28 Å [MK(62–104)] for backbone heavy atoms (N, C^{α}, C′), and 1.30 ± 0.25 Å [MK(1–59)] and 1.54 ± 0.28 Å [MK(62–104)] for all non-hydrogen atoms in the well-defined region [MK(1–59), 14–52; MK(62–104), 62–73, 77–85 and 94–104], respectively (Figures 6A and 7A).

MK(1–59) consists of three antiparallel β-strands: β_{N1} (Trp20–Pro25↑), β_{N2} (Val32–Cys39) and β_{N3} (Gln42–Val50), which are connected by two loops (Figure 6A). There is a β-bulge-like structure in β_{N1} due to Pro22 (Figure 3A). MK(62–104) also consists of three antiparallel β-strands: β_{C1} (Tyr64–Asp73), β_{C2} (Thr78–Leu85) and β_{C3} (Thr97–Thr101) (Figure 7A). The interstrand NOE pattern shows that β_{C1} contains a β-bulge at Asn68–Trp69–Gly70 (Figure 3B).

Sequence homology is observed between β_{N2} (Arg35–Glu36–Gly37–Thr38) and β_{C2} (Arg81–Gln82–Gly83–Thr84), and β_{N3} (Ile46–Arg47, Pro51–Cys52) and β_{C3} (Ile98–Arg99, Pro103–Cys104), respectively. For both MK(1–59) and MK(62–104), hydrophobic clusters are formed as shown in Figures 6B and 7B, where the 20 structures of hydrophobic residues are overlaid on the mean backbone structures of MK(1–59) and MK(62–104). The most remarkable difference in the secondary structure between MK(1–59) and MK(62–104) is the length of the second β-hairpin loop which connects the second and the third β-strands (Figure 3). It should be noted that two basic clusters are formed on the surface of MK(62–104), encircled with blue dotted lines (Figure 7C), while in MK(1–59) there are no basic clusters (Figure 6C).

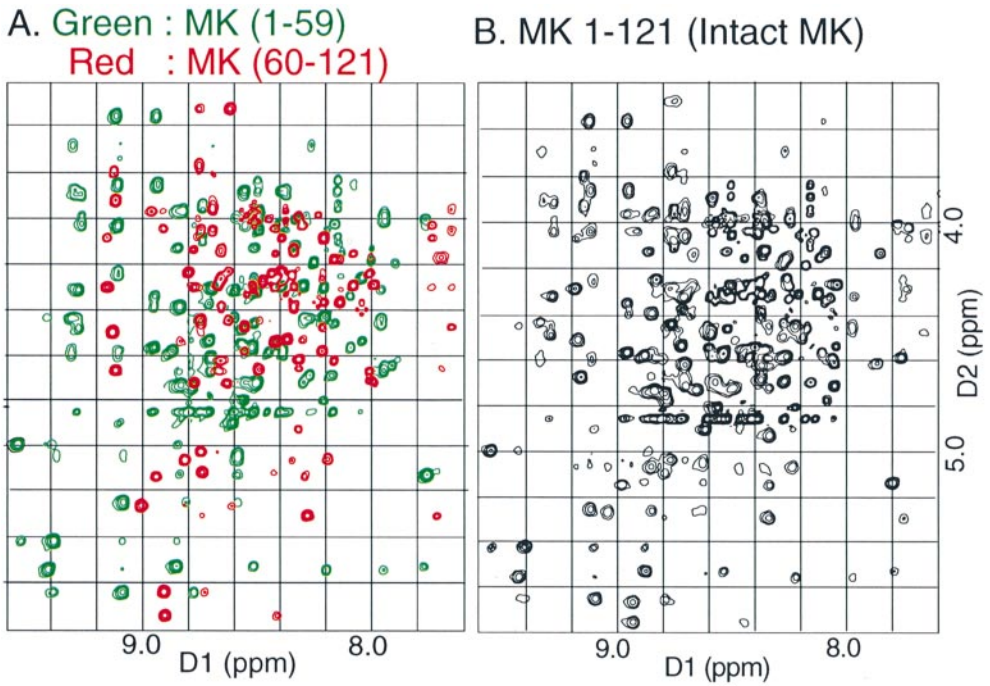

Fig. 4. Comparison of NOESY spectra of MK(1–59), MK(60–121) and MK. These spectra were measured under the same conditions (20°C, pH 6.0, 150 ms mixing time). Fingerprint regions are shown. (**A**) Superposition of NOESY spectra of MK(1–59) and MK(60–121). The spectrum of MK(1–59) is shown in green, and that of MK(60–121) in red. (**B**) NOESY spectrum of MK. Most of the peaks in (A) and (B) can be superimposed on each other.

Table I. Structural statistics of MK (1–59) and MK (62–104)

	MK (1–59)		MK (62–104)	
	20 structures	Mean structure	20 structures	Mean structure
R.m.s.ds from experimental distance constraints (Å)	0.052 ± 0.002	0.047	0.067 ± 0.002	0.071
No. of distance constraints (NOE)	(551)		(424)	
Intraresidue	224		193	
Sequential ($\|i–j\| = 1$)	137		114	
Short-range ($2 \leqslant \|i–j\| \leqslant 5$)	42		16	
Long-range ($6 \leqslant \|i–j\|$)	153		97	
Hydrogen bonds	12		0	
Dihedral angle constraints (ϕ)	5		11	
No. of distance constraint violations >0.5 Å	0–1 (max. 0.55 Å)	0 (max. 0.40 Å)	0–2 (max. 0.65 Å)	0 (max. 0.48 Å)
R.m.s.ds from experimental dihedral constraints (°)	3.79 ± 2.77	2.58	4.07 ± 1.76	3.72
No. of dihedral constraint violations >5.0°	0–2 (max. 18.5°)	0 (max. 4.9°)	0–4 (max. 19.5°)	2 (max. 9.0°)
F_{NOE} (kcal/mol)[a]	73.8 ± 6.7	60.0	94.2 ± 6.7	106.8
F_{tor} (kcal/mol)[a]	1.6 ± 1.7	0.5	3.3 ± 2.7	2.31
F_{repel} (kcal/mol)[a]	46.1 ± 5.6	33.6	37.2 ± 6.7	44.8
R.m.s.ds from idealized geometry				
Bonds (Å)	0.005 ± 0.0003 (906)	0.004	0.006 ± 0.0005 (680)	0.005
Angles (°)	0.91 ± 0.04 (1644)	0.79	0.92 ± 0.07 (1226)	0.74
Impropers (°)[b]	0.80 ± 0.06 (479)	0.62	0.87 ± 0.11 (353)	0.57

The 20 structures are the final set of dynamic simulated annealing structures; the mean structure is the structure obtained by restrained minimization of the averaged coordinate of the 20 individual structures.
[a]The value of the square-well NOE potential, F_{NOE}, is calculated with a force constant of 50 kcal/mol/Å^2. The value of F_{repel} is calculated with a force constant of 4 kcal/mol/Å^4 with van der Waal's radii scaled by a factor of 0.8 of the standard values used in the CHARMm empirical function.
[b]The improper torsion term is used to maintain the planar geometry and chirality.

Chemical shift changes of MK(62–104) upon binding to heparin 12mer

Since the major heparin-binding site of MK was located on MK(62–104) (Muramatsu *et al.*, 1994), we investigated the changes of the NMR spectra of MK(62–104) by adding an aliquot of heparin 12mer solution. Upon addition of heparin 12mer, exchange broadenings or chemical shift changes were observed for many resonances. The chemical shift changes were almost saturated at the equimolar ratio of MK(62–104) to heparin. In order to identify the residues responsible for heparin binding, we analyzed the 2D-TOCSY and 2D-NOESY spectra of MK(62–104) in the absence and presence of heparin 12mer (1:0 and 1:1.5). The chemical shift changes upon binding to heparin 12mer are shown in Figure 8A. Both the main chain and the side chain resonances of Ala88, Arg89 and Tyr90 and the side chain resonances of Lys79 and Arg81 disappeared due to exchange broadening, indicating that these residues are major heparin-binding sites. In addition, the side chain proton resonances of Trp69, Lys86, Lys87, Asn91 and Cys94 showed significant chemical shift changes of >0.15 p.p.m. There were also residues which showed appreciable chemical shift changes on the main chain amide protons but negligible shifts on the side chain resonances (Glu67, Asn68, Val80 and Leu85). The residues which showed exchange broadening or chemical shift changes of the side chain protons were plotted on the 3D structure of MK(62–104) (Figure 8B). The residues were located on the specific surface involving the positively charged clusters. There were no amino acid residues which showed appreciable shifts and/or exchange broadening on the opposite surface (Figure 8B). Thus, we confirmed that the heparin-binding surface of MK(62–104) is a major heparin-binding site in MK.

Heparin-induced oligomerization of MK molecules

Inhibition of neurite outgrowth-promoting activity of MK by heparin depends on the length of the heparin oligosaccharide chain, and the minimum heparin oligosaccharides with inhibitory activity was reported to be ~22 monosaccharide units (Kaneda *et al.*, 1996). We investigated the stoichiometry of the MK–heparin oligosaccharide complex by laser light scattering experiments. The change of solution refractive index with respect to a change in concentration of the MK–heparin complex (dn/dc) is required for the analysis of the binding stoichiometry (see Materials and methods). The (dn/dc) of MK was estimated to be 0.180 ml/g and that of heparin to be 0.134 ml/g (Arakawa *et al.*, 1994) so that the (dn/dc) of the complex was estimated from the weighted average of the molar ratio of the complex. The retention time of the gel filtration of the MK–heparin 29mer complex suggested that three MK molecules bound to the heparin 29mer. However, as the retention times of oligosaccharides are generally faster than those of proteins of the same molecular weight, the number of MK molecules which bind to one heparin 29mer molecule could be <3. We estimated the (dn/dc) of the MK–heparin 29mer complex to be within the range of 0.157–0.169 ml/g. The results of the multi-angle laser light scattering experiments for the MK complexed with 12, 20 and 29 monosaccharide units are shown in Figure 9. With the estimated (dn/dc) values, the analyses of the light scattering experiments gave the range of the molecular weight of the MK–heparin 29mer complex to be

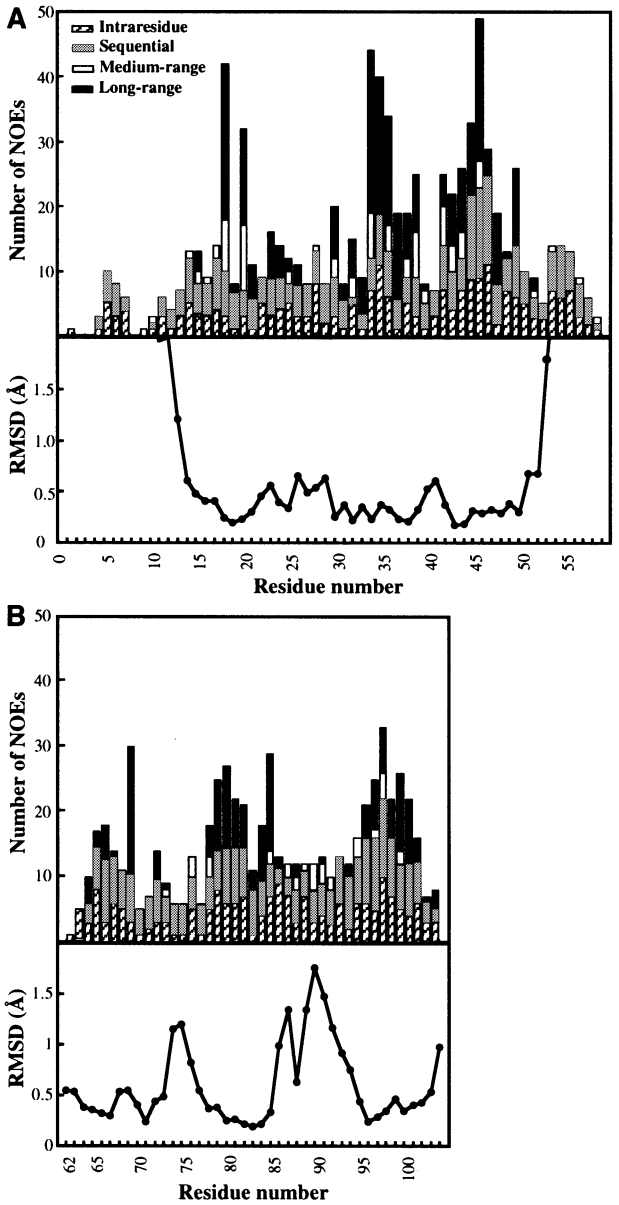

Fig. 5. Number of inter-residue NOE constraints and r.m.s.d.s for each residue of (**A**) MK(1–59) and (**B**) MK(62–104). The number of sequential distance constraints (gray bars), medium-range distance constraints with $2 \leqslant |i–j| \leqslant 5$ (open bars) and long-range distance constraints with $5 < |i–j|$ (closed bars) are shown. The average values of the main chain (N, C^{α}, C′) r.m.s.ds (●) were plotted as a function of residue number.

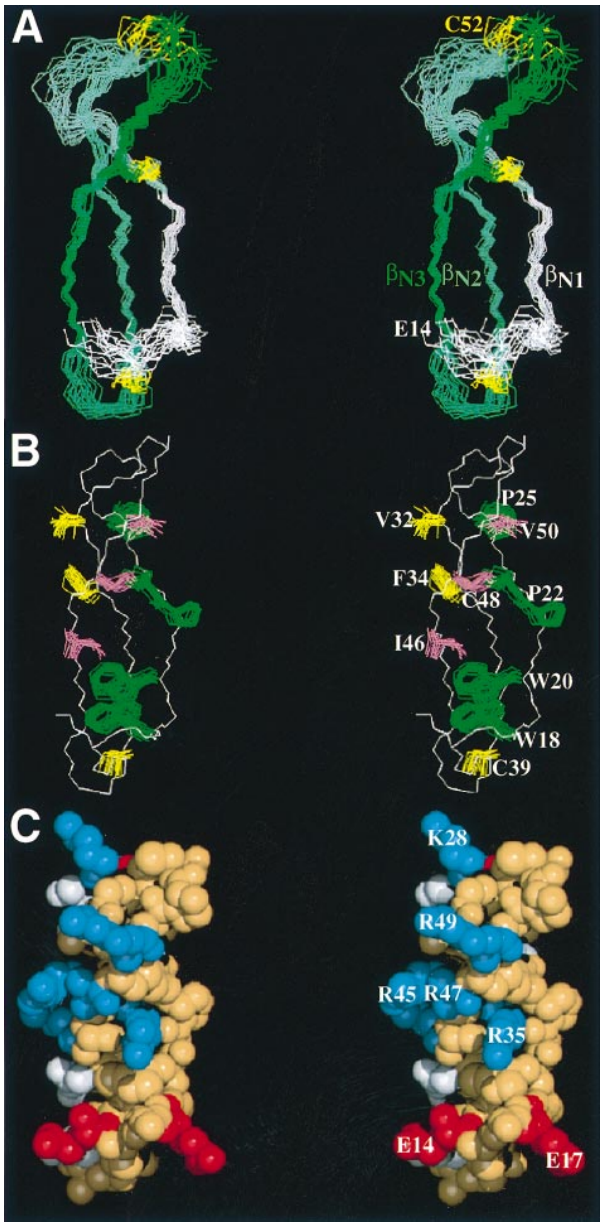

Fig. 6. Solution structures of MK(1–59) in stereo. (**A**) Main chain atoms (N, C^{α}, C′) and disulfide bonds of the 20 converged structures are superimposed. The N-terminal (Lys1–Ser13) and C-terminal (Asn53–Gly59) regions are highly disordered and are not shown. Main chain folds of each peptide from the N- to C-terminus are represented by gradation from white to green. The disulfide bonds are shown in yellow. (**B**) Hydrophobic clusters in MK(1–59). Overlays of 20 structures of the side chains for hydrophobic residues are shown on the mean structure of main chain MK(1–59). (**C**) Space filling model for MK(1–59) with annotations of basic (blue), acidic (red), hydrophobic (beige) and polar (white) residues on the surface.

33 000–36 000. This corresponds to a stoichiometry of MK:heparin 29mer of 2:1. The same analyses gave the molecular weight of the MK–heparin 20mer complex as 31 000–34 000, which was again a 2:1 stoichiometry, and that of the MK–heparin 12mer complex to be 18 000–19 000 with a 1:1 stoichiometry. The binding of MK to heparin of >20 monosaccharide units induced MK dimerization (H.Muramatsu and T.Muramatsu, unpublished results), while the binding to the heparin 12 monosaccharide units did not, showing that the inhibitory activity of heparin oligosaccharides for neuronal cell outgrowth paralleled the MK oligomerization activity.

Discussion

Structural requirement for heparin binding

The neurite outgrowth activity of MK is inhibited by addition of heparin (Kaneda *et al.*, 1996a,b). Heparin would act as an antagonist of heparan sulfate on the nerve cell surfaces and detach MK from cell surface heparan sulfate. Heparitinase digestion of target cells reduced neurite outgrouth activity, indicating that interaction of heparan sulfate with MK plays a direct role in MK-induced neurite outgrowth (Kaneda *et al.*, 1996b). Heparin-

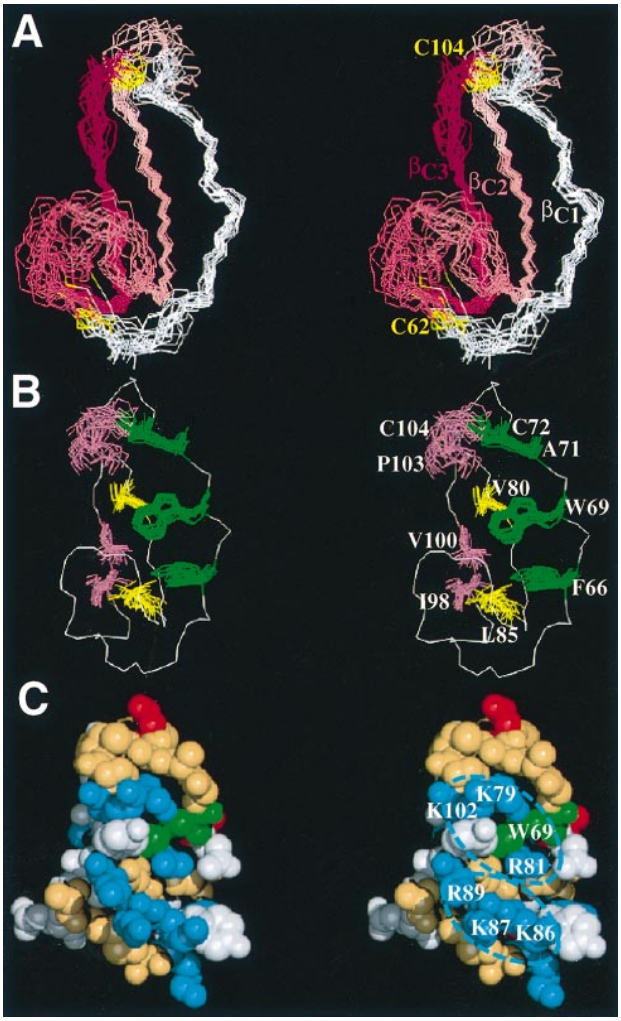

Fig. 7. Solution structures of MK(62–104) in stereo. (**A**) Main chain atoms (N, C^{α}, C′) and disulfide bonds of the 20 converged structures are superimposed. Main chain folds of each peptide from the N- to C-terminus are represented by gradation from white to red. The disulfide bonds are shown in yellow. (**B**) Hydrophobic clusters in MK(62–104). Overlay of 20 structures of the side chains for hydrophobic residues are shown on the mean structure of main chain MK(64–102). (**C**) Space filling model for MK(62–104) with annotations of basic (blue), acidic (red), hydrophobic (beige) and polar (white) residues on the surface. Trp69 is shown in green. Basic clusters are encircled by blue dotted lines.

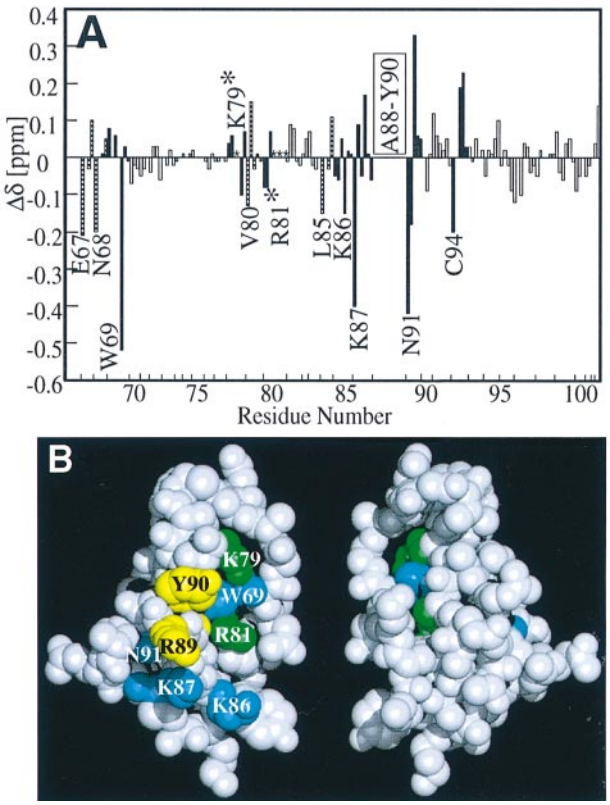

Fig. 8. Binding of MK(62–104) to heparin 12mer. (**A**) Chemical shift differences of each amino acid residue of MK(62–104) between complexed and uncomplexed forms with heparin 12mer. Striped bar, residues with only a chemical shift change of the main chain NH; closed bar, residues with chemical shift changes of >0.15 p.p.m. for side chain resonances; asterisk, residues with exchange broadening of side chain resonances. The main chain and side chain resonances of Ala88, Arg89 and Tyr90 disappear upon complex formation. (**B**) The residues with chemical shift changes of >0.15 p.p.m. for side chain resonances are shown in blue, those with exchange broadening in green, and those whose resonances disappear in yellow on the 3D structure of MK(62–104). The left structure is viewed from the same direction as in Figure 7C and the right structure shows the opposite view.

binding consensus sequences (Cardin and Weintraub, 1989) and a sequence similar to the consensus sequence are located on 2–6 (KKDKV), 85–90 (LKKARY) and 114–119 (AKKGKG) (Figure 1B). The heparin-binding activities of MK(60–121), MK(62–104) and MK(1–105) are slightly reduced compared with that of intact MK, while MK(1–59) has weak heparin-binding activity. The heparin-binding activity of MK(62–104) is dependent on the 3D structure of MK(62–104), while that of MK(1–59) is not (Muramatsu *et al.*, 1994). We will compare the structures of MK(1–59) and MK(62–104) focusing on their heparin-binding activities.

Since the main heparin-binding site is located on 62–104, the heparin-binding consensus sequence of LKKARY (85–90) may play significant roles in heparin binding. It should be noted that this sequence is located on the long hairpin loop of MK(62–104). Figure 5 shows that the loop has large r.m.s.d. values, suggesting that this region is flexible (Figure 7A). The flexibility of the long loop may be important for creating a specific heparin-binding site, as will be discussed later. This loop bends toward the β-sheet because some NOEs were observed between residues on the β-sheet and the loop (Trp69–Ala88, Leu85–Tyr90, Leu85–Asn91, Ile98–Gln95) (Figure 3B). Consequently, basic residues on the β-sheet (cluster-1; Lys79, Arg81, Lys102) and those on the long loop (cluster-2; Lys86, Lys87, Arg89) are exposed on the same surface (Figure 7C).

Titration of MK(62–104) with heparin 12mer demonstrated that cluster-1 and cluster-2 were responsible for heparin binding. The residues on the heparin-binding consensus sequence (Ala88, Arg89 and Tyr90 on cluster-2 and Lys79 and Arg81 on cluster-1) disappeared due to exchange broadening upon heparin binding, possibly forming a major heparin-binding surface (Figure 8B). On the opposite surface of MK(62–104), no residues with appreciable chemical shift change or line broadening were found, showing that this surface is not responsible for heparin-binding activity of MK (Figure 8B). Thus, we

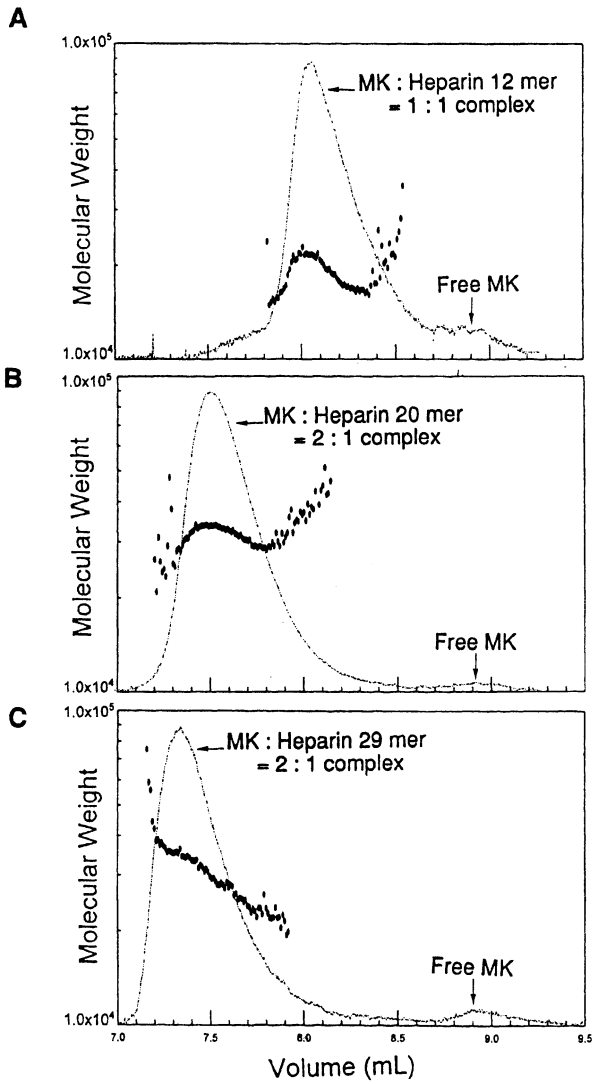

Fig. 9. Stoichiometry of MK–heparin oligosaccharide complexes. (**A**) Incubation mixtures containing 100 μl of 50 mM Tris–HCl (pH 7.4), 130 mM NaCl, 0.60 mg of MK (45 nM) and 0.04 mg of heparin 12mer units (11 nM) were applied to a gel filtration chromatograph connected to a light scattering photometer. The molecular weight of the larger peak was ~18 000; this corresponds to the molecular weight of the 1:1 complex of MK–heparin 12mer. The smaller peak corresponds to the free MK. MK has strong positive charge and many MK molecules were adsorbed by the column, so the elution peak of free MK is very small. (**B**) Analytical samples containing 0.60 mg of MK (45 nM) and 0.08 mg of heparin 20mer (11 nM) were used. (**C**) Analytical samples containing 0.60 mg of MK (45 nM) and 0.11 mg of heparin 29mer (11 nM) were used. (B) and (C) shows the molecular weights of 32 000 and 34 000, respectively, both of which correspond to MK–heparin 2:1 complex.

identified the heparin-binding surface. It is to be noted that the basic residues involved in cluster-1 and cluster-2, except for Arg89, are conserved or type-conserved in MK and HB-GAM of all the species so far examined. MK(K86Q, K87Q), where both K86 and K87 were replaced by Q86 and Q87, as well as MK(R81Q) were reported to have reduced heparin-binding and neurite outgrowth-promoting activities (Asai *et al.*, 1997). The degree of reduction of the activities was not great: the mutants had 80–85% of the heparin-binding activity of the wild-type MK. The presence of multiple amino acids interacting with heparin at each binding site as revealed in this study explains the above result: mutation of certain amino acids reduced but may not have abolished the activity of the heparin-binding site. We noted that Arg81 is located on the β-strand (β_{C2}) facing Trp69 involved in the β_{C1} bulge on the opposite strand. Both side chains of Arg81 and Trp69 direct to the same side, thus restricting the orientation of the Arg81 side chain. Therefore, the β-bulge is considered to be essential for exerting the biological function of MK.

Although MK(1–59) has many basic residues, its heparin-binding activity is weak. Unlike MK(62–104), the basic residues of MK(1–59) do not form clusters for fitting to the sulfate groups on heparin oligosaccharides (Figure 6C). There are also acidic residues on this surface, which reduce the heparin-binding activity of MK(1–59).

Dimerization of MK on heparin oligosaccharides

The MK dimer, and not the monomer, is the active form, at least in terms of enhancement of plasminogen activator activity of endothelial cells (Kojima *et al.*, 1997). We propose here a molecular model for dimer formation of MK on heparin oligosaccharides (Figure 10). We show the heparin with 20 monosaccharide units, consisting of basic disaccharide repeat units comprised of L-iduronic acid (Idu) and D-glucosamine (GlcN) joined by a β1–4 linkage. The conformations of heparin are shown as helical, as derived from NMR studies (Mulloy *et al.*, 1993), where Idu rings are assumed to have either the $^1C_4$ chair conformation or the $^2S_0$ skew boat conformation (Figure 10A and C). It should be noted that when MK(62–104) binds to heparin to form a dimer in a head-to-head manner, a fused heparin-binding surface is formed between the interface of the two MK(62–104) molecules (Figure 10A). This binding surface is formed by basic residue clusters (cluster-2; Lys86, Lys87, Arg89) on the long hairpin loop. The flexible nature of this loop is suitable for sandwiching a sulfate cluster on heparin. The interval of exposed positively charged clusters on the dimer surface (circled with a dotted blue line in Figure 10A) is almost the same as those of sulfate group clusters on heparin (circled with a dotted pink line in Figure 10A). The size and the form of these clusters on the dimer surface and those of the sulfate clusters on heparin oligosaccharide fit well with each other. These features imply that MK dimer would bind heparin more strongly than monomer. Light scattering experiments clarified the number of MK molecules bound to heparin oligosaccharides. Heparin 12mer, which was shown to bind to one molecule of MK, is unable to inhibit MK-dependent neurite outgrowth, while heparin 20 and 29mer, which should bind to two molecules of MK, inhibit neurite outgrowth (Kaneda *et al.*, 1996). MK probably also acts as a dimer in neurite outgrowth, and heparin oligosaccharides >20mer may prevent heparan sulfate binding on the cell surface of MK and thus inhibit neurite outgrowth. Heparin has two negatively charged surfaces where the sulfate groups line both sides of the chain (Figure 10C). Two binding forms are considered: (i) N- and C-terminal halves align on the same negatively charged surface of heparin, or (ii) the N- and C-terminal halves bind to the opposite surfaces of heparin. The latter model is consistent with the fact that one MK molecule binds to the heparin 12 monosaccharide units since there

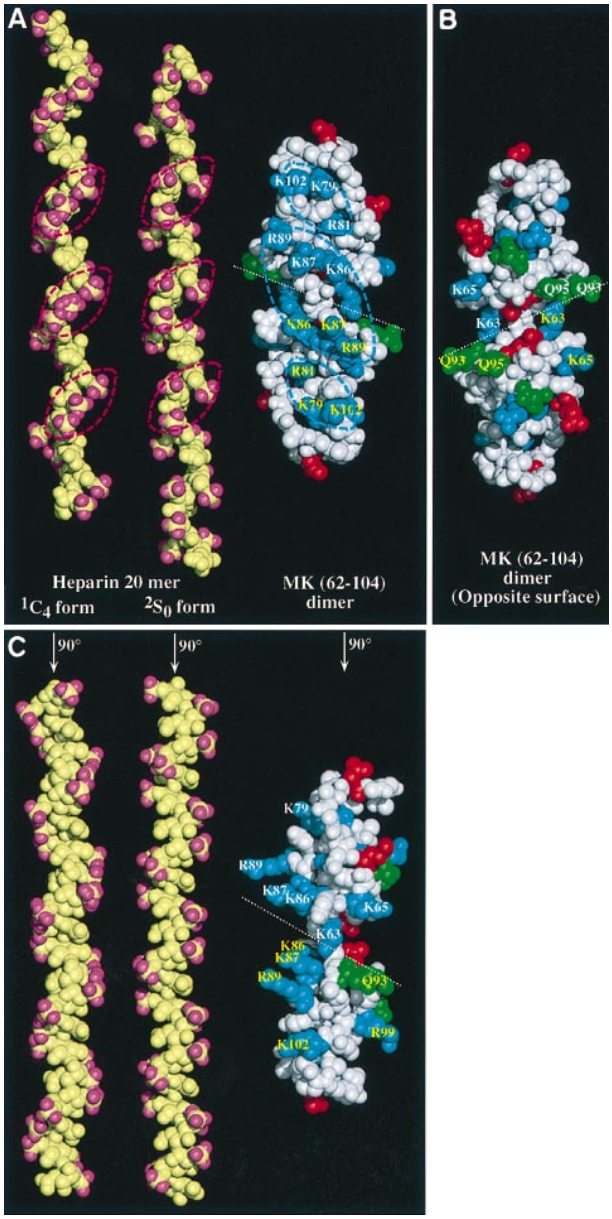

Fig. 10. The model for binding of MK(62–104) dimer on the heparin 20mer units with two conformations. (**A**) The model for heparin and MK(62–104) head-to-head dimer complex (blue, basic residues; red, acidic residues; green, Gln; and pink, oxygens of sulfate groups). Positively charged clusters (blue dotted circles) of MK(62–104) fit to negatively charged clusters (pink dotted circles) of heparin. (**B**) The opposite surface of MK(62–104) to that shown in (A). The acidic residues of MK(62–104) are localized opposite the heparin-binding surface. Gln95 which is attacked by transglutaminase is exposed opposite to the heparin-binding surface and is in close proximity to Lys63 on the counterpart. Lys63 is thought to be an amine donor in the transglutaminase reaction. (**C**) Side view of (A). The sulfate groups are localized on the right and left sides of the heparin molecule. Basic charged clusters in MK(62–104) dimer fit the clusters of sulfate groups.

is no space for MK to bind to heparin 12mer with alignment of the N- and C-terminal halves on the same surface.

The linker region (Asn53–Asp61) which connects the N- and C-terminal halves seems to be long enough to link the two domains bound on the opposite surface of the heparin oligosaccharide chain. Though Phe55 of mouse MK (which corresponds to Phe58 of human MK) in the linker is cleaved by chymotrypsin, the proteolysis is inhibited specifically in the presence of heparin (Matsuda *et al.*, 1996). This result as well as the NOESY spectra suggest that the linker is flexible and exposed in heparin-free form. However, in heparin-bound form, the linker may bind to the heparin chain and may be protected from proteolysis.

Dimerization of MK by transglutaminase

The proposed model for the MK–heparin complex is supported by the cross-linking experiments with transglutaminase. Upon incubation with transglutaminase, MK formed an oligomer through cross-linkages. The oligomer formation was significantly enhanced in the presence of heparin. Furthermore, when MK(60–121) was treated with transglutaminase, Gln95 in MK(60–121) was reported to serve as an amine acceptor in the cross-linking reaction (Kojima *et al.*, 1997). According to our model (Figure 10B), Gln95 is exposed on the surface opposite to the heparin-binding site, so that binding to heparin does not block the access of transglutaminase. It should be noted that Gln95 in MK(62–104) is located in close proximity to Lys63 on its counterpart when the head-to-head dimer is formed, thus explaining the hyperreactivity of MK towards cross-linkage by transglutaminase.

If the oligomerization of MK by transglutaminase is inhibited, the plasminogen activator-enhancing activity is abolished (Kojima *et al.*, 1997). Though it has not been determined whether or not transglutaminase acts on MK *in vivo*, this result also suggests that the heparin-induced oligomerization of MK is important for MK activity. MK oligomerization may cause receptor oligomerization and activation. The signal transducing MK receptor has not been identified, but a candidate is a receptor-type tyrosine phosphatase: the extracellular domain of receptor-type tyrosine phosphatase β is known to bind strongly to HB-GAM (Maeda *et al.*, 1996). The 3D structure of MK presented here may be helpful in pinpointing amino acid residues important for interaction with the putative signal transducing receptor.

Materials and methods

Materials

MK, MK(1–59), MK(60–121) and MK(62–104) were chemically synthesized by solution procedure (Inui *et al.*, 1996). Heparin oligosaccharides were prepared from porcine intestine (Kaneda *et al.*, 1996).

NMR measurements

MK, MK(1–59), MK(60–121) and MK(62–104) were dissolved at 3 mM in D_2O or H_2O (10% D_2O). The pH was adjusted to an uncorrected glass electrode reading of 6.0 for MK, MK(1–59) and MK(60–121) and 5.0 for MK(62–104) by addition of aliquots of 1 M DCl and NaOD using a Radiometer PHM86 pH meter. No extra salt was added to the samples. ^{1}H NMR spectra were recorded on a 600 MHz Varian UNITYplus 600 spectrometer at a probe temperature of 20°C for MK, MK(1–59), MK(60–121) and MK(62–104). Sodium 2,2-dimethyl-2-silapentane-5-sulfonate (DSS) was added as an internal chemical shift standard. DQF-COSY (Rance *et al.*, 1983), TOCSY with 40 and 75 ms mixing times using the clean MLEV17 sequences (Cavanaugh and Rance, 1992) and two-dimensional NOESY with 75, 100 and 150 ms mixing times (Jeener *et al.*, 1979; Macura *et al.*, 1981) were recorded in the phase-sensitive mode. The water resonance was suppressed by selective irradiation during the relaxation delay or by water flip-back. A total of 64 or 128 scans were accumulated for each t_1 with a relaxation delay of 1.3 s. All two-dimensional spectra were recorded with 512 (t_1)×1024 (t_2) data points and with a spectral width of 7500 Hz. After

zero filling once in the t_2 dimension and twice in the t_1 dimension, phase-shifted sine-bell functions were applied prior to Fourier transformation. A total of 2048×2048 real data matrices were finally obtained, and digital resolution was 3.7 Hz/point in both dimensions.

Structure calculations

Interproton distance constraints were derived from NOE cross-peak intensities (peak height) in the NOESY spectra (75 or 100 ms mixing time) according to the method of Hatanaka *et al.* (1994). The peak intensities were translated into distance on the basis of the relationship (NOE intensity) ∝ (distance)$^{-6}$ and standard known distances of sequential $d_{\alpha N}$ in β-sheet = 2.2 Å in H_2O NOESY and interstrand $d_{\alpha\beta}$ in antiparallel β-sheet = 2.3 Å in D_2O NOESY. The upper-bound distance constraints were the calculated distance plus 0.5 Å. The lower-bound distance constraints were set to 1.8 Å. Dihedral angle constraints were obtained based on the analysis of DQF-COSY (Wagner *et al.*, 1987). The 3D structures were calculated by the simulated annealing method with X-PLOR v3.1 using distance constraints. A final set of 20 converged structures was selected from 100 calculations on the basis of agreement with the experimental data and the van der Waal's energy. A mean structure was obtained by averaging the coordinates of the structures that were superimposed in advance to the best converged structure, and then minimized under the constraints (Clore *et al.*, 1986).

Measurement of the stoichiometry of MK–heparin oligosaccharide complexes

A DAWN DSP multi-angle laser light scattering photometer (Wyatt Technology) at 632.8 nm and a refractive index detector (Shodex) at 632.8 nm were used to measure the molecular weight of MK–heparin oligosaccharide complexes. For analytical experiments, MK was incubated at room temperature for 1.5 h with appropriate heparin oligosaccharides in the elution buffer. The light scattering photometer was connected after a gel filtration chromatography with a PROTEIN KW-802.5 (Shodex) column. We used an elution buffer of 50 mM Tris–HCl (pH 7.4), containing 130 mM NaCl (Maccarana *et al.*, 1993; Kinnunen *et al.*, 1996) at a flow rate of 0.4 ml / min.

The light scattering data were analyzed in the following manner.

$$\frac{(K\cdot c)}{R(\theta)} = \frac{1}{Mw\cdot P(\theta)} + 2A_2\cdot c + \ldots \quad (1)$$

$$K = 4\pi^2 n^2 \left(\frac{dn}{dc}\right) \lambda_0{}^4 N_A \quad (2)$$

where c is the concentration in g/ml, $R(\theta)$ is the light scattering intensity at angle θ, Mw is the molecular weight, A_2 is the second Virial constant, n is the reflective index, (dn/dc) is a change of solution refractive index with respect to a change in concentration of the MK–heparin complex and N_A is Avogadro's constant. P (θ) is the scattering factor which depends on the average square rotation radius, $\langle r_g{}^2\rangle$. P (θ) is the function of $\sin^2$ (θ/2) and

$$\lim_{\theta \to 0} P(\theta) = 1 \quad (3)$$

Therefore, from Equation 1, we find

$$\lim_{\substack{c \to 0 \\ \theta \to 0}} \frac{K\cdot c}{R(\theta)} = \frac{1}{Mw} \quad (4)$$

Practically, $Kc/R(\theta)$ versus $\sin^2$ (θ/2) (Zimm plot) is plotted and is extrapolated to $\sin^2$ (θ/2) = 0. Then, the intercept gives Mw, and the slope gives $\langle r_g{}^2\rangle$.

References

Adachi,Y. *et al.* (1996) Midkine as a novel target gene for Wilms tumor suppressor gene (WTI). *Oncogene*, **13**, 2197–2203.

Arakawa,T., Wen,J. and Philo,J.S. (1994) Stoichiometry of heparin binding to basic fibrobrast growth factor. *Arch. Biochem. Biophys*., **308**, 267–273.

Aridome,K., Tsutsui,J., Takao,S., Kadomatsu,K., Ozawa,M., Aikou,T. and Muramatsu,T. (1995) Increased midkine gene expression in human gastrointestinal cancers. *Jap. J. Cancer Res*., **118**, 88–93.

Asai,T., Watanabe,K., Kojima,S., Ichihara-Tanaka,K., Kaneda,N., Iguchi,A., Inagaki,F. and Muramatsu,T. (1997) Heparin binding sites in midkine; identification and analysis of their different roles in neurite guidance and in enhancement of plasminogen activator activity. *Biochem. Biophys. Res. Commun*., **236**, 66–70.

Cardin,A.D. and Weintraub,H.J.R. (1989) Molecular modeling of protein–glycosaminoglycan interactions. *Arterioclerosis*, **9**, 21–32.

Cavanagh,J. and Rance,M. (1992) Suppression of cross-relaxation effects in TOCSY spectra via a modified DISPI-2 mixing sequence. *J. Magn. Resonance*, **96**, 670–678.

Chauhan,A.K., Li,Y.S. and Deuel,T.F. (1993) Pleiotrophin transfoms NIH3T3 cells and induces tumors in nude mice. *Proc. Natl Acad. Sci. USA*, **90**, 679–682.

Clore,G.M., Brünger,A.T., Karplus,M. and Gronenborn,A.M. (1986) Application of molecular dynamics with interproton distance restraints to three-dimensional protein structure determination. *J. Mol. Biol*., **191**, 523–551

Czubayko,F., Schulte,A.M., Berchem,G.J. and Wellstein,A. (1996) Melanoma angiogenesis and metastasis modulated by ribozyme targeting of the secreted growth factor pleiotrophin. *Proc. Natl Acad. Sci. USA*, **93**, 14753–14758.

Fabri,L., Nice,E.C., Ward,L.D., Maruta,H., Burgess,A.W. and Simpson,R.J. (1992). Characterization of bovine heparin-binding neurotrophic factor (HBNF)—assignment of disulfide bonds. *Biochem. Int*., **28**, 1–9.

Fabri,L., Maruta,H., Muramatsu,H., Muramatsu,T., Simpson,R.J., Burgess,AW. and Nice,E.C. (1993) Structural characterization of native and recombinant forms of the neurotrophic cytokine MK. *J. Chromatogr*., **646**, 213–226.

Hatanaka,H., Oka,M., Kohda,D., Tate,S., Suda,A., Tamiya,N. and Inagaki,F. (1994) Tertiary structure of erabutoxin b in aqueous solution as elucidated by two-dimensional nuclear magnetic resonance. *J. Mol. Biol*., **240**, 155–166.

Inui,T. *et al.* (1996) Solution synthesis of human midkine, a novel heparin-binding neurotrophic factor consisting of 121 amino acid residues with five disulfide bonds. *J. Peptide Sci*., **2**, 28–39.

Jeener,J., Meier,B.H., Bachmann,P. and Ernst,R.R. (1979) Investigation of exchange processes by two-dimesional NMR spectroscopy. *J. Chem. Phys*., **71**, 4546–4553.

Kadomatsu,K., Tomomura,M. and Muramatsu,T. (1988) cDNA cloning and sequencing of a new gene intensely expressed in early differentiation stages of embryonal carcinoma cells and in mid-gestation period of mouse embryogenesis. *Biochem. Biophys. Res. Commun*., **151**, 1312–1318.

Kadomatsu,K., Huang,R.-P., Suganuma,T., Murata,F. and Muramatsu,T. (1990) A retinoic acid responsive gene MK found in the teratocarcinoma system is expressed in spatially and temporally controlled manner during mouse embryogenesis. *J. Cell Biol*., **110**, 607–616.

Kadomatsu,K., Hagihara,M., Akhter,S., Fan,Q.-W., Muramatsu,H. and Muramatsu,T. (1997) Midkine induces the transformation of NIH3T3 cells. *Br. J. Cancer*, **75**, 354–359.

Kaneda,N., Talukder,A.H., Ishihara,M., Hara,S., Yoshida,K. and Muramatsu,T. (1996a) Structural characteristics of heparin-like domain required for interaction of midkine with embryonic neurons. *Biochem. Biophys. Res. Commnun*., **220**, 108–112.

Kaneda,N., Talukder,A.H., Nishiyama,H., Koizumi,S. and Muramatsu,T. (1996b) Midkine, a heparin-binding growth/differentiation factor, possesses nerve cell adhesion and guidance activity for neurite outgrowth *in vitro*. *J. Biochem*., **119**, 1150–1156.

Kinnunen,T., Raulo,E., Nolo,R., Maccarana,M., Lindahl,U. and Rauvala,H. (1996) Neurite outgrowth in brain neurons induced by heparin-binding growth-associated molecule (HB-GAM) depends on the specific interaction of HB-GAM with heparan sulfate at the cell surface. *J. Biol. Chem*., **271**, 2243–2248.

Kojima,S., Muramatsu,H., Amanuma,H. and Muramatsu,T. (1995a) Midkine enhances fibrinolytic activity of bovine endothelial cells. *J. Biol. Chem*., **270**, 9590–9596.

Kojima,S., Inui,T., Kimura,T., Sakakibara,S., Muramatsu,H., Amanuma,H., Maruta,H. and Muramatsu,T. (1995b) Synthetic peptides derived from midkine enhances plasminogen activator in bovine aortic endothelial cells. *Biochem. Biophys. Res. Commun*., **206**, 468–473.

Kojima,S., Inui,T., Muramatsu,H., Kimura,T., Sakakibara,S. and Muramatsu,T. (1995c) Midkine is a heat and acid stable polypeptide capable of enhancing plasminogen activator activity and neurite outgrowth extension. *Biochem. Biophys. Res. Commun*., **216**, 574–581.

Kojima,S. *et al.* (1997) Dimerization of midkine by transglutaminase and its functional implication. *J. Biol. Chem*., **202**, 9410–9416.

Kurtz,A., Schulte,A.M. and Wellstein,A. (1995) Pleiotrophin and midkine in normal development and tumor biology. *Crit. Rev. Oncogen.*, **6**, 151–171.

Li,Y.S., Milner,P.G., Chauhan,A.K., Watson,M.A., Hoffman,R.M., Kodner,C.M., Milbrant,J. and Deuel,T.F. (1990) Cloning and expression of a developmentally regulated protein that induces mitogenic and neurite outgrowth activity. *Science*, **250**, 1690–1694.

Lindhal,U., Lindholt,K., Spillmann,D. and Kjellen,L. (1991) More to heparin than anticoagulation. *Thromb. Res*., **75**, 1–32.

Maccarana,M., Casu,B. and Lindahl,U. (1993) Minimal sequence in heparin/heparan sulfate required for binding of basic fibroblast growth factor. *J. Biol. Chem*., **268**, 23898–23905.

Macura,S., Huang,Y., Suter,D. and Ernst,R.R. (1981) Two-dimensional chemical exchange and cross-relaxation spectroscopy of coupled nuclear spins. *J. Magn. Resonance*, **43**, 259–281.

Maeda,N., Nishiwaki,T., Hamanaka,H. and Noda,M. (1996) 6B4 proteoglycan/phosphacan, an extracellular variant of receptor-like protein-tyrosine phosphatase 5 (RPTPβ) binds pleiotrophin/heparin binding growth associated-molecule (HB-GAM). *J. Biol. Chem*., **271**, 21446–21452.

Mahoney,S.-A., Perry,M., Seddon,A., Bohlen,P. and Haynes,L. (1996) Transglutaminase forms midkine homodimers in cerebellar neurons and modulates its neurite-outgrowth response. *Biochem. Biophys. Res. Commun*., **224**, 147–152.

Matsuda,Y., Talukder,A.H., Ishihara,M., Hara,S., Yoshida,K., Muramatsu,T. and Kaneda,N. (1996) Limited proteolysis by chymotrypsin of midkine and inhibition by heparin binding. *Biochem. Biophys. Res. Commun*., **228**, 176–181.

Matsumoto,K., Wanaka,A., Takatsuji,K., Muramatsu,H., Muramatsu,T. and Tohyama,M. (1994) A novel family of heparin-binding growth factors, pleiotrophin and midkine are expressed in the developing rat cerebral cortex. *Dev. Brain Res*., **79**, 229–241.

Merenmies,J. and Rauvala,H. (1990) Molecular cloning of the 18kDa growth-associated protein of developing brain. *J. Biol. Chem*., **265**, 16721–16724.

Michikawa,M., Xu,R.Y., Muramatsu,H., Muramatsu,T. and Kim,S.U. (1993a) Midkine is a mediator of retinoic acid induced neuronal differentiation of embryonal carcinoma cells. *Biochem. Biophys. Res. Commun*., **192**, 1312–1318.

Michikawa,M., Kikuchi,S., Muramatsu,H., Muramatsu,T. and Kim,S.U. (1993b) Retinoic acid responsive gene product, midkine (MK), has neurotrophic functions for mouse spinal cord and dorsal root ganglion neurons in culture. *J. Neurosci. Res*., **35**, 530–539.

Mitsiadis,T.A., Salmivirta,M., Muramatsu,T., Muramatsu,H., Rauvala,H., Lehtonen,E., Jalkanen,M. and Thesleff,I. (1995a) Expression of the heparin-binding cytokines, midkine (MK) and HB-GAM (pleiotrophin) is associated with epithelial–mesenchymal interactions during fetal development and organonesis. *Development*, **121**, 37–51.

Mitsiadis,T.A., Muramatsu,T., Muramatsu,H. and Thesleff,I. (1995b) Midkine (MK), a heparin-binding growth/differentiation factor, is regulated by retinoic acid and epithelial–mesenchymal interactions in the developing mouse tooth, and affects cell proliferation and morphogenesis. *J. Cell Biol*., **129**, 267–281.

Mulloy,B., Forster,M.J., Jones,C. and Davis,D.B. (1993) N.m.r. and molecular-modelling studies of the solution conformation of heparin. *Biochem. J*., **293**, 849–858.

Muramatsu,H., Shirahama,H., Yonezawa,S., Maruta,H. and Muramatsu,T. (1993) Midkine (MK), a retinoic acid-inducible growth/differentiation factor: immunochemical evidence for the function and distribution. *Dev. Biol*., **159**, 392–402.

Muramatsu,H., Inui,T., Kimura,T., Sakakibara,S., Song,X., Maruta,H. and Muramatsu,Y. (1994) Localization of heparin-binding, neurite outgrowth and antigenic regions in midkine molecule. *Biochem. Biopys. Res. Commun*., **203**, 1131–1139.

Muramatsu,T. (1994). The midkine family of growth/differentiation factors. *Dev. Growth Differ*., **36**, 1–8.

Nakagawara,A., Milbrandt,J., Muramatsu,T., Deuel,T.F., Zhao,H., Cnaan,A. and Brodeur,G.M. (1995) Differential expression of pleiotrophin and midkine in advanced neuroblastomas. *Cancer Res*., **55**, 1792–1797.

O'Brien,D., Cranston,D., Fuggle,S., Bicknell,R. and Harris,A.L. (1996) The angiogenic factor midkine is expressed in bladder cancer, and overexpression correlates with a poor outcome in patients with invasive cancers. *Cancer Res*., **56**, 2515–2518.

Peng,H.B., Ali,A.A., Dai,Z., Daggett,D.F., Raulo,E. and Rauvala,H. (1995). The role of heparin-binding growth-associated molecule (HB-GAM) in the postsynaptic induction in cultured muscle cells. *J. Neurosci*., **15**, 3027–3038.

Rance,M., Sørensen,O.W., Bodenhausen,G., Wagner,G., Ernst,R.R. and Wüthrich,K. (1983) Improved spectral resolution in COSY proton NMR spectra of proteins via double quantum filtering. *Biochem. Biophys. Res. Commun*., **117**, 479–485.

Raulais,D., Lagente-Chevallier,O., Guettet,C., Duprez,D., Courtois,Y. and Vigny,M. (1991) A new heparin-binding protein regulated by retinoic acid from chick embryos. *Biochem. Biophys. Res. Commun*., **174**, 708–715.

Raulo,E., Chernousov,M.A., Carey,D.J., Nolo,R. and Rauvala,H. (1994) Isolation of a neural cell surface receptor of heparin binding growth-associated molecule (HB-GAM). *J. Biol. Chem*., **269**, 12999–13004.

Rauvala,H. (1989) An 18-kd heparin-binding protein of developing brain that is distinct from fibroblast growth factors. *EMBO J*., **8**, 2933–2941.

Ruoslahti,E. and Yamaguchi,Y. (1991) Proteoglycans as modulator of growth factor activites. *Cell*, **64**, 867–869.

Schulte,A.M., Lai,S., Kartz,A., Czubayko,F., Riegel,A.T. and Wellstein,A. (1996) Human trophoblast and choricarcinoma expression of the growth factor pleiotrophin attributable to germ-line insertion of an endogeneous retrovirus. *Proc. Natl Acad. Sci. USA*, **93**, 14759–14764.

Spivak-Kroizman,T. *et al*. (1994) Heparin-induced oligomerization of FGF molecules is responsible for FGF receptor dimerization, activation and cell proliferation. *Cell*, **79**, 1015–1024.

Tomomura,M., Kadomatsu,K., Matsubara,S. and Muramatsu,T. (1990) A retinoic acid-responsive gene, MK, found in the teratocarcinoma system. Heterogeneity of the transcript and the nature of the translation product. *J. Biol. Chem*., **265**, 10765–10770.

Tsutsui,J., Kadomatsu,K., Matsubara,S., Nakagawara,A., Hamanoue,M., Takao,S., Shimazu, H., Ohi,Y. and Muramatsu,T. (1993) A new family of heparin-binding growth differentiation factors: increased midkine expression in Wilms' tumor and other human carcinomas. *Cancer Res*., **53**, 1281–1285.

Unoki,K., Ohba,N., Arimura,H., Muramatsu,H. and Muramatsu,T. (1994) Rescue of photoreceptors from the damaging effects of constant light by midkine, a retinoic acid responsive gene product. *Invest. Ophthalmol. Vis. Sci*., **35**, 4063–4068.

Yayon,A., Klagsbrun,M., Esko,J.D., Leder,P. and Ornitz,D.M. (1991) Cell surface heparin-like molecules are required for binding of bFGF to its high affinity receptor. *Cell*, **64**, 841–848.

Yoshida,Y., Goto,M., Tsutsui,J., Ozawa,M., Sato,E., Osame,M. and Muramatsu,T. (1995) Midkine is present in the early stage of cerebral infarct. *Dev. Brain Res*., **85**, 25–30.

Wagner,G., Braun,W., Havel,T.F., Schaumann,T., Go,N. and Wüthrich,K. (1987) Protein structures in solution by nuclear magnetic resonance and distance geometry. The polypeptide fold of the basic pancreatic trypsin inhibitor determined using two different algorithms, DISGEO and DISMAN. *J. Mol. Biol*., **196**, 611–639.

Wüthrich,K. (1986) *N.M.R. of Proteins and Nucleic Acids*. John Wiley and Sons, New York.

Received on May 6, 1997; revised on September 9, 1997